Decreased CSF clearance and increased brain amyloid in Alzheimer's disease

yi li (liyi73@gmail.com)
Weill Cornell Medical College https://orcid.org/0000-0002-3875-3513

Henry Rusinek
NYU Langone Medical Center: NYU Langone Health

Tracy Butler
Weill Cornell Medical College: Weill Cornell Medicine

Lidia Glodzik
Weill Cornell Medical College: Weill Cornell Medicine

Elizabeth Pirraglia
NYU Langone Medical Center: NYU Langone Health

John Babich
Weill Cornell Medical College: Weill Cornell Medicine

P. David Mozley
Weill Cornell Medical College: Weill Cornell Medicine

Sadek Nehmeh
Weill Cornell Medical College: Weill Cornell Medicine

Silky Pahlajani
Weill Cornell Medical College: Weill Cornell Medicine

Xiuyuan Wang
Weill Cornell Medical College: Weill Cornell Medicine

Emily B. Tanzi
Weill Cornell Medical College: Weill Cornell Medicine

Liangdong Zhou
Weill Cornell Medical College: Weill Cornell Medicine

Sara Strauss
Weill Cornell Medical College: Weill Cornell Medicine

Roxana Carare
University of Southampton

Neil Theise
NYU Langone Medical Center: NYU Langone Health

Nobuyuki Okamura
Tohoku Medical and Pharmaceutical University: Tohoku Ika Yakka Daigaku

Mony J. de Leon

Weill Cornell Medical College: Weill Cornell Medicine

Research

Keywords: Alzheimer's disease (AD), brain amyloid-beta (Aβ), brain glymphatic clearance (BGC), F-THK5331, MRI, PET

Posted Date: September 20th, 2021

DOI: https://doi.org/10.21203/rs.3.rs-900478/v1

Version of Record: A version of this preprint was published at Fluids and Barriers of the CNS on March 14th, 2022. See the published version at https://doi.org/10.1186/s12987-022-00318-y.

Abstract

In sporadic Alzheimer's disease (AD), brain amyloid-beta (Aβ) deposition is believed to be a consequence of impaired Aβ clearance, but this relationship is not well established in living human subjects. CSF clearance, a major feature of brain glymphatic clearance (BGC), has been shown to be abnormal in AD murine models. Prior MRI phase contrast studies have reported reduced aqueductal CSF flow in AD. Using PET and tau tracer ^{18}F-THK5117, we previously reported that the ventricular CSF clearance of the PET tracer was reduced in AD and associated with elevated brain Aβ levels. In the present study, using two PET tracers, ^{18}F-THK5351 and ^{11}C-PiB to estimate CSF clearance, we observe that the ventricular CSF clearance measures were correlated ($r = .66$, $p < .01$), with reductions in AD of 18 and 27%, respectively. We also replicated a significant relationship between ventricular CSF clearance (^{18}F-THK5331) and brain Aβ load ($r = -.64$, $p < .01$). With a larger sample size, we extended our observations to show that reduced CSF clearance is associated with reductions in cortical thickness and cognitive performance. Overall, the findings support the hypothesis that failed CSF clearance is a feature of AD that is related to Aβ deposition and to the pathology of AD. Longitudinal studies are needed to determine whether failed CSF clearance is a predictor of progressive amyloidosis or its consequence.

One Sentence Summary

CSF clearance is impaired in mild AD and inversely related to brain Aβ deposition, and related to cognative function and cortical thickness.

Introduction

Two decades after it was hypothesized that the amyloidosis of sporadic Alzheimer's disease (AD) is mechanistically related to the impaired clearance of Aβ [1,2], there is limited understanding of the pathophysiology of brain Aβ clearance in sporadic AD [3–5]. Part of the difficulty relates to the absence of direct, non-invasive methods to examine the role of human CSF as a carrier of Aβ and other waste molecules. Human lumbar spine CSF sampling studies with $^{13}C_6$-leucine have demonstrated a systemic Aβ clearance deficit in AD in the context of unchanged Aβ production [6]. Murine studies have revealed a brain glymphatic clearance system where waste products including Aβ are carried in the interstitial fluid (ISF) and CSF [7–9] and drain into immune modulated dural lymphatics [10]. In transgenic AD models, these clearance deficits are progressive [11].

Neuroimaging, including MRI and PET and computational fluid dynamics analysis have been employed to investigate the glymphatic transport function in the live animal and human brain [12]. Dynamic contrast enhanced magnetic resonance imaging (DCE-MRI) showed potential to tracking glymphatic solute and fluid transport in the CNS with both intrathecal and intravenous Gd-DOTA injection [13–16]. Several quantification methods of the glymphatic clearance utilize the CSF and brain signal changes in dynamic PET [15,17,18]. We previously observed that ventricular CSF clearance was reduced in AD and inversely related to the magnitude of brain Aβ deposits measured using ^{11}C-PiB [17]. In the present study,

a larger sample and a different tracer, ^{18}F-THK5351, were used to measure CSF clearance. In each subject, ^{11}C-PiB was used to measure the amyloid burden, and MRI to estimate brain atrophy. Our results with ^{18}F-THK5351 radiotracer replicate the prior AD clearance reductions and the association of these clearance deficits with Aβ lesions. We report for the first time that the magnitude of CSF clearance is inversely related to decreased cortical thickness and to decreased cognitive function.

Materials And Methods

Study Participants: 24 elderly subjects (age range 61–90 y, 10 male and 14 female) participated in this IRB approved study. Written informed consent was obtained from each participant or their legal caretakers. Participants included 9 normal controls (NL) and 15 AD subjects including 6 very mild cases (CDR = 0.5) and 9 with mild to moderate cognitive symptoms (CDR ≥ 1.0) [19] [20]. All subjects showed amyloid deposits in cerebral cortex with global PiB uptake ratio greater than 1.25 [21]. AD patients were recruited from the memory clinic of Tohoku University Hospital. The controls were recruited from the general community. Subject diagnoses were made at a consensus conference according to the National Institute of Neurological and Communicative Disorders and Stroke/AD and Related Disorders Association criteria [22]. All participants received standardized clinical and neuropsychological assessments, including CDR, MMSE and ADAS-cog.

PET and MRI Image Acquisition: Each study participant received within a 3-month interval, the clinical assessments, a high resolution T1-weighted MRI, and two dynamic PET exams, one exam performed with ^{18}F-THK5351 tracer used to estimate CSF clearance and the other with ^{11}C-PiB- for Aβ. The syntheses of ^{18}F-THK5351 and ^{11}C-PiB compounds were previously described [23] [24]. PET imaging was performed using an Eminence STARGATE PET-CT scanner (Shimadzu, Kyoto, Japan). On separate days, subjects received an intravenous injection of ^{18}F-THK5351 (185 MBq), or ^{11}C-PiB (296 MBq). Dynamic PET data were obtained in list mode for 60 min for ^{18}F-THK5351 and 70 min for ^{11}C-PiB. Images tracking the time course of ^{18}F-THK5351 and ^{11}C-PiB exams were reconstructed to a 128 x 128 x 79 matrix of 2 x 2 x 2.6 mm voxels in 26 time frames for ^{18}F-THK5351 and 25 frames for ^{11}C-PiB. MR images were obtained using a SIGNA 1.5 tesla unit (General Electric, Milwaukee, WI). The MRI protocol included a 3D volumetric acquisition of a T1-weighted gradient echo sequence with parameters: echo time/repetition time 2.4/50 ms; flip angle 45°; acquisition matrix 256 × 256; 1 excitation; field of view 22 cm; and a 2.0 mm slice thickness without gaps.

MRI Segmentation: FreeSurfer software (v. 6.1) was used for MRI brain segmentation [25]. Regions of Interest (ROIs) were determined for the neocortical gray matter (GM) and white matter (WM), the cerebellar gray matter, and the combined left + right lateral ventricle [26]. The whole brain ROI was derived from FreeSurfer aparc + aseg file [27] which includes the complete cerebral and cerebellar volume and pons. The average thickness of the neocortical GM was used as an index of brain atrophy. Statistical Parametric Mapping (SPM 12) software (www.fil.ion.ucl.ac.uk/spm) was used to calculate the total intracranial volumes. To optimize CSF sampling from the lateral ventricle and minimize partial volume

contamination by brain tissue, an eroded lateral ventricle mask ELVM was created using the 4 mm 3D erosion of MRI-segmented ventricles. Both ^{18}F-THK5351 and ^{11}C-PiB scans have been visually examined, and no choroid plexus binding was observed with both tracers.

PET Image Workflow: After decay correction, standardized uptake value (SUV) time-framed images were created by normalizing the reconstructed radioactivity by injected dose and body weight. To minimize the effect of head motion for each subject, the dynamic PET frames were realigned to the first-time frame using SPM. The anatomically segmented MR images were co-registered separately to the space of the ^{18}F-THK5351 and ^{11}C-PiB PET scans using SPM12. Satisfactory inter-modality alignment was verified for each exam by an experienced neuroradiologist. Each PET time frame was partial volume corrected (PVC) using a modified one tissue model [28].

Estimations of PET tracer clearance: Ventricular CSF, whole brain and blood time activity curves (TAC) were derived for each participant. Tracer concentrations in the blood were sampled from the internal carotid artery, guided by MR scans that were co-registered to the PET data [29]. Blood TAC reached a peak within 2 min and approached low asymptotic time course by 4 min (Fig. 1a). Brain TACs reached a peak between 2 and 4 minutes after injection of tracer. The ventricular CSF clearance was derived from the slope of a linear regression fit of SUV(t) for ELVM (see MRI segmentation section) over 10–30 min [30]. The 10–30 min time frame was selected to minimize the potential contribution of blood in the choroid plexus. To control for the variability in the amount of radiotracer delivered to the brain across subjects, the slope was normalized by the total brain SUV of the tracer over the first 4 minutes after injection. To facilitate data interpretation and avoid dealing with negative quantities, the absolute value of the clearance slope was used. The resulting normalized absolute value slope was denoted as vCSF-SLOPE and used throughout this study to estimate CSF clearance rate.

PET SUVr Estimations of brain amyloid: The amyloid binding of cerebral grey matter was estimated using ^{11}C-PiB binding based on the 50–70 min interval, as we reported previously[31]. The uptake period with the cerebellar gray matter was used as the reference tissue in the standardized uptake value ratio (SUVr).

Statistical Analysis: The general linear model and univariate analysis of variance (ANOVA), with Tukey post hoc tests, were used to examine the vCSF-SLOPE across the NL and AD clinical groups. All significant results were confirmed using the nonparametric Mann–Whitney test with Bonferroni corrections for multiple comparisons. The relationships between the vCSF-SLOPE and Aβ binding, cortical thickness and cognitive function were tested using parametric correlation models, and nonparametric correlation models were tested if the the data was not normally distributed. The ventricular volume and age were tested as covariates in our regressions. All statistical tests were two-sided and significance was set at $p < .05$. All analyses were checked for violations of the model assumptions, and no conflicts were found.

Results

Clinical data: The demographic data from the NL and AD groups are shown in Table 1. There were no age or gender differences by group. The ADAS-cog and MMSE were significantly different in AD subjects as compared with NL (ADAS-cog: $F = 21.1$ $p < .01$, MMSE: $F = 23.5$ $p < .01$).

Table 1
Participant demographic data

	N	age	Gender(M/F)	MMSE*	ADAS-cog*
NL	9	72.8 (8.9)	3/6	28.8(1.3)	4.8 (2.2)
AD	15	76.3 (8.9)	7/8	21.9(4.3)	16.5 (7.1)
Values are expressed as mean (SD); *p < .0.01, between NL and AD groups.					

Clearance derived from ^{18}F-THK5351 and ^{11}C-PiB tracers

Group vCSF Clearance Effect

Both ^{18}F-THK5351 and ^{11}C-PiB tracers showed significantly lower vCSF-SLOPE in AD as compared with NL. The $vCSF\text{-}SLOPE_{THK5351}$ was reduced in AD by 20% ($F = 10.2$, $p < .01$). The $vCSF\text{-}SLOPE_{PiB}$ was reduced by 28% in AD ($F = 24.4$, $p < .01$, see Table 2). The findings remained significant after PVC ($p < .01$ for all).

Within subject vCSF: Across the entire sample, the $vCSF\text{-}SLOPE_{THK5351}$ and $vCSF\text{-}SLOPE_{PiB}$ were closely associated ($r = .66$, $p < .01$, $n = 24$, see Fig. 2). The correlation remained significant when the analysis was restricted to the AD group ($r = .61$, $p < .05$, $n = 15$).

The effects of CSF clearance on cortical thickness and the tracer binding

Group Tracer Binding Effects. The PiB PET examined within the 50–70 min SUVr showed significantly higher (46%) GM binding in AD as compared with NL (see Table 2). We also tested both tracers for binding during the interval when clearance measurements were made. From 10–30 min a PiB GM SUVr binding effect was observed in the AD group, significantly higher (by 22%, $p < .01$) than in NL. However, at 10–30 min, the difference in THK5331 SUVr, higher by 5% in AD vs NL, was not significant ($p > .05$).

Table 2
vCSF-SLOPE and tracer binding

Group	vCSF-SLOPE$_{THK5351}$	vCSF-SLOPE$_{PiB}$	^{11}C-PiB GM SUVr 50–70 min	^{11}C-PiB GM SUVr 10–30 min	^{18}F-THK5351 GM SUVr 10–30 min
NL	.11(.02)	.11(.01)	1.28(0.17)	1.02(0.05)	1.30(0.12)
AD	.09(.02)	.08(.02)	1.88(0.30)	1.25(0.12)	1.37(0.10)
Diff. from normal	-18%, p < .01	-27%, p < .01	46%, p < .01	22%, p < .01	5%, NS

The relationship between vCSF clearance and amyloid binding. Across all subjects, the vCSF-SLOPE$_{THK5351}$ was inversely correlated with the Aβ GM binding (r=-.64, p < .01, n = 24, see Fig. 3). This correlation remained significant after PVC (r=-.72, n = 24, p < .01). Importantly, the relationship between vCSF-SLOPE and Aβ GM binding remained significant when restricted to the AD group (r = −.58, n = 15, p < .05). The relationship between vCSF-SLOPE and GM Aβ binding was not significant in the NL group (p > .05).

The relationship of CSF clearance and cortical thickness. The vCSF-SLOPE$_{THK5351}$ was positively correlated with the cerebral cortex thickness (r = .55, n = 24, p < .01). The correlation was a trend when restricted to the AD group (r = .45, n = 15, p = .08), reaching p < .05 significance in a one-tailed test. However, it was not significant in the NL group.

CSF Clearance, Ventricular Volume and age: To rule out ventricular size and age as confounds for the vCSF-SLOPE measure, we examined the ventricular volume and age as covariates in our regressions. We observed that for the total group the correlation between vCSF-SLOPE$_{THK5331}$ and Aβ GM binding remained significant after adjustment for the age and ventricular size (r = −.44, p < .05, n = 24). In an analysis restricted to the AD group, this relationship remained significant even after controlling for the age and ventricular size (r=-.56, n = 15, p < .05).

CSF clearance vs tracer binding and cognitive performance

Over all subjects, the vCSF clearance was inversely correlated with the ADAS-cog (vCSF-SLOPE$_{THK5351}$ r=-.55, p < .01, n = 24). Studying the clinical groups separately showed that only in the NL group did the association of vCSF-SLOPE$_{THK5351}$ and ADAS-cog remain significant (r=-.83, n = 9, p < 0.01). Over all subjects, the PiB tracer binding in GM was also correlated with the ADAS-cog (r = .77, p < .01, n = 24). Studying the two groups separately showed that only in the AD group did the association of the PiB tracer GM binding and ADAS-cog remain significant (r = .58, n = 15, p < .05).

Discussion

The impaired clearance of CSF in AD: The impaired clearance of Aβ and the impaired clearance of the CSF and ISF that drains the Aβ from the brain has been suspected for many years as playing a role in the deposition of Aβ in the AD brain [32–35]. Abnormalities in several physiological clearance mechanisms that potentially underlie Aβ removal from the brain have been shown in animal models. These include clearance across the BBB [36], enzymatic degradation [37–39], perivascular Aβ lesions affecting ISF bulk flow [40], reduced glymphatic paravascular clearance in AD-Tg mice [7], lymphatic and immune related clearance failures [10], and defects in CSF absorption [41].

Prior MRI phase contrast studies have shown reduced CSF flow at the acqueduct in AD as compared to mild cognitive impairment (MCI) [42] and associated with cognitive deficits [43]. However, the phase contrast method directly measures pulsatile velocity rather than the flow and the results are highly variable across studies [44, 45]. Intrathecal MR contrast studies directly show CSF flow and the glymphatic transport of Gd-DTPA through the brain parenchyma [46, 47]. While dynamic contrast MRI appears to be more precise in evaluating the CSF clearance function, the intrathecal administration of contrast is more invasive and it has limited application in clinical practice. Compared to these MRI measures, our dynamic PET measure reflects tracer removal rate from the ventricle, which appears to more directly reflect the rate of CSF clearance.

PET studies show that small molecular weight PET tau and amyloid tracers demonstrate rapid brain penetrance and clearance, with over 70% of the injected dose cleared from the brain by the study end [48–50]. We exploited this feature in our studies as a potential CSF clearance biomarker [17]. Previously we reported in a small sample that ventricular CSF clearance is reduced in AD and inversely associated with brain Aβ levels. Now, using THK533, another radiotracer, and with a larger sample, we report a replication of our prior findings. Moreover, we report for the first time correlations between CSF clearance and brain atrophy and cognitive functioning as related to AD.

Recent transgenic AD mouse studies have demonstrated age-related reductions in ISF and CSF clearance as well as CSF clearance deficits prior to Aβ accumulation [7, 51]. In humans, using a $^{13}C_6$-leucine labelled Aβ and continuous lumbar spine CSF sampling, Bateman et al. observed that Aβ clearance was reduced 33% in AD but the Aβ production rate was unaffected [3, 6]. Consistent with Bateman et al., we observed a 20% reduction relative to NL group when CSF clearance was measured with ^{18}F-THK5331 and 28% when measured with ^{11}C-PiB PET.

The present study replicates and extends our prior report that impaired human CSF clearance can be estimated in vivo using dynamic PET imaging [17]. We estimated the overall CSF clearance rate by quantifying the rate of change in tracer in lateral ventricles. With similar reasoning, Silverberg et al. used an invasive method with a ventricular catheter to test the hypothesis that impaired CSF dynamics were associated with AD (Silverberg et al., 2001). They estimated the CSF production rate using intrathecal pressure changes before and after a volume of CSF was removed. However, this method is invasive, and a method that does not perturb the very system that is being measured would be preferable. With our minimally invasive PET technique, we observed close relationships between the magnitude of reduced

CSF clearance and an increased brain Aβ burden, the loss of brain tissue, and reduced memory performance.

Impaired CSF clearance and brain amyloid: Our dynamic PET data suggest ventricular CSF clearance could be a useful marker to monitor the CSF flow dysfunctions. Overall, our results are consistent with prior evidence showing that the increased residence time of Aβ contributes to its aggregation and fibrillization in the extracellular space [52]. We find reduced CSF clearance in AD for both THK5331 and PiB PET radiotracers. Moreover, the clearance measures were significantly correlated ($r = .66$, $n = 24$, $p < .01$) cross tracers. It is important to consider that the CSF flow is highly correlated across tracers even though the magnitude of brain binding is four-fold greater for the PiB tracer than for the THK5331 tracer. This supports the validity of the method and point towards a preference to the THK5331 for clearance estimations. Further highlighting the value of the method, the clearance correlation with the amyloid burden was seen in the total group as well separately within the AD group.

^{18}F-THK5351 was developed as tau tracer, but off-target binding to Monoamine oxidase B has been reported, thus invalidating the tau specificity. Consequently, we did not use the THK5331 to estimate the tau burden. Therefore, it remains untested whether CSF clearance is related to tau binding. Other more selective tau tracers are now under investigation, which may establish the relationshiop between CSF clearance and brain tau binding.

The PiB tracer, which also demonstrated utility as a CSF clearance agent, appears to be partially confounded by disease-sensitive binding detectable in the time frame used to estimate CSF clearance. We believe this is reflected in the greater PiB clearance 27% vs 18% for THK5331, since some of the PiB tracer enters Aβ plaques even in the initial 10–30 min time window. Overall, as compared with PiB, THK53351 has an advantage as a clearance agent.

Impaired CSF clearance is associated with decreased cognitive function: The CSF clearance measure and the brain amyloid binding were both associated with cognitive function. Intriguingly, in the subgroups analysis, the association of CSF clearance and cognitive function was significant in the NL group($r=-.83$, $n = 9$, $p < 0.01$), while the correlation between brain amyloid binding and cognitive function was significant in the AD group ($r = .58$, $n = 15$, $p < .05$). These data suggest that the CSF clearance measure could have potential in the early disease stages to serve as a biomarker to monitor prelesion disease progression. In the absence of longitudinal data, this remains speculative. Nevertheless, this observation agrees with a previous animal study that showed clearance deficits prior to Aβ lesions [7].

Confounds and study limitations: ventricular CSF clearance could be confounded by both specific and non-specific binding of the tracer in the brain. However, our tests suggest that for the time interval studied, a relative independence of clearance and binding effects for THK5331. This is supported by the observation that ^{18}F-THK5351, unlike ^{11}C-PiB, did not show binding effect at the 10–30 min time interval. Additional evidence justifying that tracer brain binding has a negligible effect on CSF clearance rate is based on the high within-subject correlations for ^{18}F-THK5351 and PiB ($r = .66$, $p < 0.01$), even though the

tracers have different binding distribution volumes [53, 54]. Precise quantification would require using a radiotracer that has no known binding profile while retaining a profile of rapid blood-CSF-brain barrier penetrance and clearance [55]. Overall, the results suggest that brain tracer binding had limited effect on vCSF-SLOPE for ^{18}F-THK5331 and ^{11}C-PiB.

We evaluated several other possible confounds, including choroid plexus binding and partial-volume errors. Neither tracer showed choroid plexus binding that could potentially bias the ventricular clearance estimates. The ventricular partial volume error, due to contamination by proximity to brain, was minimized by individually sampling the ventricle 4 mm from the brain and with subsequent partial volume corrections [56]. Partial volume correction did not change the results. Another possible confound, the enlarged ventricular volume in AD may cause tracer dilution, thereby altering the clearance function. This was also tested and fount not to affect our findings.

Overall, our cross-sectional findings are consistent with the hypothesis that CSF turnover reductions are found in AD. Moreover, these data support a mechanism whereby Aβ is deposited in brain due to reductions in CSF clearance [3, 35]. However, a longitudinal sample is needed for estimating the directionality of the relationship between impaired clearance and brain Aβ deposits.

Declarations

Ethics approval and consent to participate: The protocol was approved by the Ethics Committee of Tohoku University Hospital.

Availability of data and materials: The datasets analyzed during the current study are available from the corresponding author on request.

Acknowledgments: The authors would also like to thank Dr. Louisa Bokacheva for review this manuscript.

Funding: This study was supported by NIH/NIA grants AG057848, RF1AG057570, R56 AG058913, AG022374, AG013616, AG012101, T32AG052909-01A1, NIH-HLB HL111724 and HL118624. The work at Tohoku University was supported by Health and Labor Sciences research grants from the Ministry of Health, Labor, and Welfare of Japan, a Grant-in-Aid for Scientific Research (B) (23390297), a Grant-in-Aid for Scientific Research on Innovative Areas (26117003), a grant from the Japan Advanced Molecular Imaging Program (J-AMP) of the Ministry of Education, Culture, Sports, Science and Technology, and the research fund from GE Healthcare and Sumitomo Electric Industries, Ltd.

Author contributions: YL, MdeL, and HR designed and conducted the study. NO, HY, LZ contributed to the acquisition of the imaging data and its interpretation LG, TB, GB, JB, P. DM, SN, SP, ET, SS, RC, NT contributed to data interpretation, LP was responsible for the statistical analyses

Competing interests: The authors declare that they have no competing interests.

References

1. Shibata M, Yamada S, Kumar SR, Calero M, Bading J, Frangione B, et al. Clearance of Alzheimer's amyloid-ss(1–40) peptide from brain by LDL receptor-related protein-1 at the blood-brain barrier. JClinInvest. 2000;106:1489–99.
2. Hardy J, Selkoe DJ. The amyloid hypothesis of Alzheimer's disease: progress and problems on the road to therapeutics. Science. 2002;297:353–6.
3. Mawuenyega KG, Sigurdson W, Ovod V, Munsell L, Kasten T, Morris JC, et al. Decreased clearance of CNS beta-amyloid in Alzheimer's disease. Science. 2010;330:1774.
4. Hawkes CA, Jayakody N, Johnston DA, Bechmann I, Carare RO. Failure of perivascular drainage of beta-amyloid in cerebral amyloid angiopathy. Brain Pathol. 2014;24:396–403.
5. Jack CR Jr, Bennett DA, Blennow K, Carrillo MC, Dunn B, Haeberlein SB, et al. NIA-AA Research Framework: Toward a biological definition of Alzheimer's disease. Alzheimers Dement. 2018;14:535–62.
6. Bateman RJ, Munsell LY, Morris JC, Swarm R, Yarasheski KE, Holtzman DM. Human amyloid-beta synthesis and clearance rates as measured in cerebrospinal fluid in vivo. NatMed. 2006;12:856–61.
7. Iliff JJ, Wang M, Liao Y, Plogg BA, Peng W, Gundersen GA, et al. A paravascular pathway facilitates CSF flow through the brain parenchyma and the clearance of interstitial solutes, including amyloid beta. SciTranslMed. 2012;4:147ra111.
8. Nedergaard M. Neuroscience. Garbage truck of the brain. Science. 2013;340:1529–30.
9. Louveau A, Smirnov I, Keyes TJ, Eccles JD, Rouhani SJ, Peske JD, et al. Structural and functional features of central nervous system lymphatic vessels. Nature. 2015;523:337–41.
10. Da Mesquita S, Papadopoulos Z, Dykstra T, Brase L, Farias FG, Wall M, et al. Meningeal lymphatics affect microglia responses and anti-Aβ immunotherapy. Nature. Nature Publishing Group; 2021;1–6.
11. Nedergaard M, Goldman SA. Glymphatic failure as a final common pathway to dementia. Science. 2020;370:50–6.
12. Benveniste H, Lee H, Ozturk B, Chen X, Koundal S, Vaska P, et al. Glymphatic Cerebrospinal Fluid and Solute Transport Quantified by MRI and PET Imaging. Neuroscience [Internet]. 2020 [cited 2021 Aug 5]; Available from: https://www.sciencedirect.com/science/article/pii/S0306452220307302.
13. Deike-Hofmann K, Reuter J, Haase R, Paech D, Gnirs R, Bickelhaupt S, et al. Glymphatic Pathway of Gadolinium-Based Contrast Agents Through the Brain: Overlooked and Misinterpreted. Invest Radiol. 2019;54:229–37.
14. Dyke JP, Xu HS, Verma A, Voss HU, Chazen JL. MRI characterization of early CNS transport kinetics post intrathecal gadolinium injection: Trends of subarachnoid and parenchymal distribution in healthy volunteers. Clin Imaging. 2020;68:1–6.
15. Elkin R, Nadeem S, Haber E, Steklova K, Lee H, Benveniste H, et al. GlymphVIS: Visualizing Glymphatic Transport Pathways Using Regularized Optimal Transport. In: Frangi AF, Schnabel JA,

Davatzikos C, Alberola-López C, Fichtinger G, editors. Medical Image Computing and Computer Assisted Intervention – MICCAI 2018. Cham: Springer International Publishing; 2018. pp. 844–52.

16. Taoka T, Jost G, Frenzel T, Naganawa S, Pietsch H. Impact of the Glymphatic System on the Kinetic and Distribution of Gadodiamide in the Rat Brain: Observations by Dynamic MRI and Effect of Circadian Rhythm on Tissue Gadolinium Concentrations. Invest Radiol. 2018;53:529–34.
17. de Leon MJ, Li Y, Okamura N, Tsui WH, Saint-Louis LA, Glodzik L, et al. Cerebrospinal fluid clearance in Alzheimer Disease measured with dynamic PET. JNuclMed. 2017;58:1471–6.
18. Schubert JJ, Veronese M, Marchitelli L, Bodini B, Tonietto M, Stankoff B, et al. Dynamic 11C-PiB PET Shows Cerebrospinal Fluid Flow Alterations in Alzheimer Disease and Multiple Sclerosis. J Nucl Med. 2019;60:1452–60.
19. Morris JC, Rubin EH. Clinical diagnosis and course of Alzheimer's disease. Psychiatr Clin North Am. 1991;14:223–36.
20. Morris JC, McManus DQ. The neurology of aging: normal versus pathologic change. Geriatrics. 1991;46:47–8, 51–4.
21. Farrell ME, Jiang S, Schultz AP, Properzi MJ, Price JC, Becker JA, et al. Defining the Lowest Threshold for Amyloid-PET to Predict Future Cognitive Decline and Amyloid Accumulation. Neurology. 96: Wolters Kluwer Health, Inc. on behalf of the American Academy of Neurology; 2021. pp. e619–31.
22. McKhann GM, Knopman DS, Chertkow H, Hyman BT, Jack CR Jr, Kawas C, et al. The diagnosis of dementia due to Alzheimer's disease: Recommendations from the National Institute on Aging-Alzheimer's Association workgroups on diagnostic guidelines for Alzheimer's disease. Alzheimer's Dementia. 2011;7:263–9.
23. Harada R, Furumoto S, Tago T, Katsutoshi F, Ishiki A, Tomita N, et al. Characterization of the radiolabeled metabolite of tau PET tracer 18F-THK5351. EurJNuclMedMolImaging. 2016;43:2211–8.
24. Verdurand M, Bort G, Tadino V, Bonnefoi F, Le Bars D, Zimmer L. Automated radiosynthesis of the Pittsburg compound-B using a commercial synthesizer. NuclMedCommun. 2008;29:920–6.
25. Fischl B, van der Kouwe A, Destrieux C, Halgren E, Segonne F, Salat DH, et al. Automatically parcellating the human cerebral cortex. CerebCortex. 2004;14:11–22.
26. Li Y, Tsui W, Rusinek H, Butler T, Mosconi L, Pirraglia E, et al. Cortical laminar binding of PET amyloid and tau tracers in Alzheimer disease. JNuclMed. 2015;56:270–3.
27. Baker SL, Maass A, Jagust WJ. Considerations and code for partial volume correcting [18F]-AV-1451 tau PET data. Data Brief. 2017;15:648–57.
28. Meltzer CC, Leal JP, Mayberg HS, Wagner HN Jr, Frost JJ. Correction of PET data for partial volume effects in human cerebral cortex by MR imaging. JComputAssistTomogr. 1990;14:561–70.
29. Su Y, Blazey TM, Snyder AZ, Raichle ME, Hornbeck RC, Aldea P, et al. Quantitative amyloid imaging using image-derived arterial input function. PLoS One. 2015;10:e0122920.
30. Zou KH, Tuncali K, Silverman SG. Correlation and Simple Linear Regression. Radiology Radiological Society of North America. 2003;227:617–28.

31. Li Y, Rinne JO, Mosconi L, Pirraglia E, Rusinek H, DeSanti S, et al. Regional analysis of FDG and PIB-PET images in normal aging, mild cognitive impairment, and Alzheimer's disease. Eur J Nucl Med Mol Imaging. 2008;35:2169–81.
32. May C, Kaye JA, Atack JR, Schapiro MB, Friedland RP, Rapoport SI. Cerebrospinal fluid production is reduced in healthy aging. Neurology. 1990;40:500–3.
33. Shibata M, Yamada S, Kumar SR, Calero M, Bading J, Frangione B, et al. Clearance of Alzheimer's amyloid-ss(1–40) peptide from brain by LDL receptor-related protein-1 at the blood-brain barrier. JClinInvest. 2000;106:1489–99.
34. Silverberg GDH. The cerebrospinal fluid production rate is reduced in dementia of the Alzheimer's type. Neurol. 2001;57:1763–6.
35. Tarasoff-Conway JM, Carare RO, Osorio RS, Glodzik L, Butler T, Fieremans E, et al. Clearance systems in the brain-implications for Alzheimer disease. NatRevNeurol. 2015;11:457–70.
36. Zlokovic BV. Neurovascular pathways to neurodegeneration in Alzheimer's disease and other disorders. NatRevNeurosci. 2011;12:723–38.
37. Aston-Mourney K, Zraika S, Udayasankar J, Subramanian SL, Green PS, Kahn SE, et al. Matrix metalloproteinase-9 reduces islet amyloid formation by degrading islet amyloid polypeptide. JBiolChem. 2013;288:3553–9.
38. Farris W, Mansourian S, Chang Y, Lindsley L, Eckman EA, Frosch MP, et al. Insulin-degrading enzyme regulates the levels of insulin, amyloid beta-protein, and the beta-amyloid precursor protein intracellular domain in vivo. ProcNatlAcadSciUSA. 2003;100:4162–7.
39. Miners JS, Baig S, Palmer J, Palmer LE, Kehoe PG, Love S. Abeta-degrading enzymes in Alzheimer's disease. Brain Pathol. 2008;18:240–52.
40. Weller RO, Galea I, Carare RO, Minagar A. Pathophysiology of the lymphatic drainage of the central nervous system: Implications for pathogenesis and therapy of multiple sclerosis. Pathophysiology. 2010;17:295–306.
41. Pollay M. The function and structure of the cerebrospinal fluid outflow system. Cerebrospinal Fluid Res. 2010;7:9-8454-7–9.
42. El Sankari S, Gondry-Jouet C, Fichten A, Godefroy O, Serot JM, Deramond H, et al. Cerebrospinal fluid and blood flow in mild cognitive impairment and Alzheimer's disease: a differential diagnosis from idiopathic normal pressure hydrocephalus. Fluids Barriers CNS. 2011;8:12.
43. Attier-Zmudka J, Sérot J-M, Valluy J, Saffarini M, Macaret A-S, Diouf M, et al. Decreased Cerebrospinal Fluid Flow Is Associated With Cognitive Deficit in Elderly Patients. Frontiers in Aging Neuroscience. 2019;11:87.
44. Luetmer PH, Huston J, Friedman JA, Dixon GR, Petersen RC, Jack CR, et al. Measurement of Cerebrospinal Fluid Flow at the Cerebral Aqueduct by Use of Phase-contrast Magnetic Resonance Imaging: Technique Validation and Utility in Diagnosing Idiopathic Normal Pressure Hydrocephalus. Neurosurgery. 2002;50:534–43.

45. Stoquart-ElSankari S, Balédent O, Gondry-Jouet C, Makki M, Godefroy O, Meyer M-E. Aging Effects on Cerebral Blood and Cerebrospinal Fluid Flows. J Cereb Blood Flow Metab. 27: SAGE Publications Ltd STM; 2007. pp. 1563–72.
46. Eide PK, Ringstad G. MRI with intrathecal MRI gadolinium contrast medium administration: a possible method to assess glymphatic function in human brain. Acta Radiologica Open SAGE Publications. 2015;4:2058460115609635.
47. Iliff JJ, Lee H, Yu M, Feng T, Logan J, Nedergaard M, et al. Brain-wide pathway for waste clearance captured by contrast-enhanced MRI. J Clin Invest American Society for Clinical Investigation. 2013;123:1299–309.
48. Mathis CA, Bacskai BJ, Kajdasz ST, McLellan ME, Frosch MP, Hyman BT, et al. A lipophilic thioflavin-T derivative for positron emission tomography (PET) imaging of amyloid in brain. BioorgMedChemLett. 2002;12:295–8.
49. Okamura N, Furumoto S, Harada R, Tago T, Yoshikawa T, Fodero-Tavoletti M, et al. Novel 18F-labeled arylquinoline derivatives for noninvasive imaging of tau pathology in Alzheimer disease. JNuclMed. 2013;54:1420–7.
50. Harada R, Furumoto S, Tago T, Katsutoshi F, Ishiki A, Tomita N, et al. Characterization of the radiolabeled metabolite of tau PET tracer 18F-THK5351. EurJNuclMedMolImaging. 2016;43:2211–8.
51. Kress BT, Iliff JJ, Xia M, Wang M, Wei HS, Zeppenfeld D, et al. Impairment of paravascular clearance pathways in the aging brain. AnnNeurol. 2014;76:845–61.
52. Hardy JA, Higgins GA. Alzheimer's disease: the amyloid cascade hypothesis. Science. 1992;256:184–5.
53. Mintun MA, Larossa GN, Sheline YI, Dence CS, Lee SY, Mach RH, et al. 11C]PIB in a nondemented population: potential antecedent marker of Alzheimer disease. Neurology. 2006;67:446–52.
54. Harada R, Okamura N, Furumoto S, Furukawa K, Ishiki A, Tomita N, et al. 18F-THK5351: A novel PET radiotracer for imaging neurofibrillary pathology in Alzheimer Disease. JNuclMed. 2016;57:208–14.
55. Waterhouse NN, Kothari PJ, Dooley M, Hu B, de Leon MJ, Babich J, et al. Synthesis of [1-11C]Butanol via a facile solid phase extraction protocol. Appl Radiat Isot. 2020;159:109078.
56. Muller-Gartner HW, Links JM, Prince JL, Bryan RN, McVeigh E, Leal JP, et al. Measurement of radiotracer concentration in brain gray matter using positron emission tomography: MRI-based correction for partial volume effects. JCerebBlood Flow Metab. 1992;12:571–83.

Figures

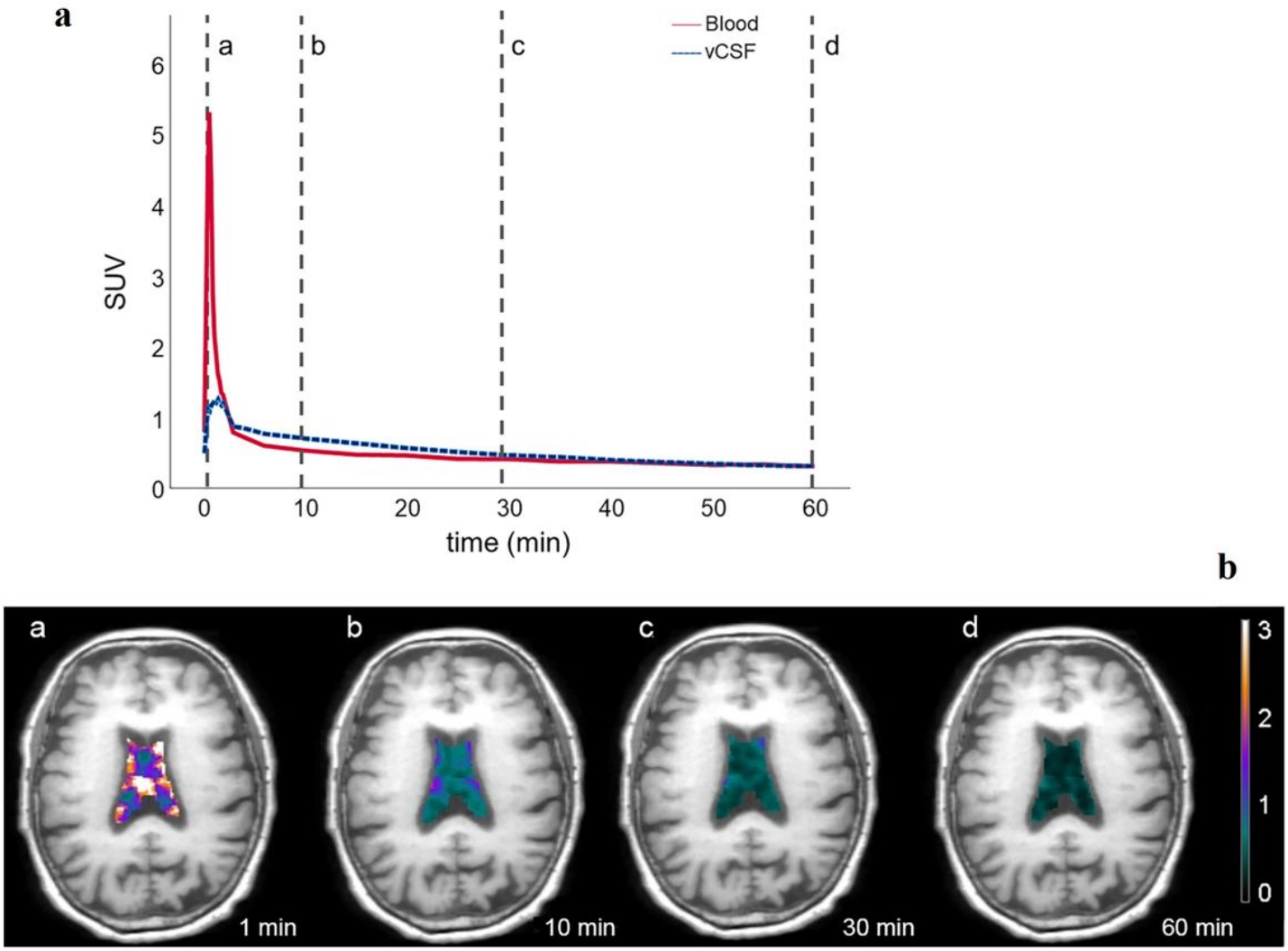

Figure 1

a. Ventricular CSF(t) time activity curve and the image-derived 18F-THK5351 arterial blood curve, averaged over all subjects. The tracer in blood reached peak approximately within 2 min after injection. The lines marked a, b, c, d correspond to the sampled time points for vCSF-SLOPE and to the four time frames shown in Fig.1b. b. The four images from one AD subject demonstrate the changes in 18F-THK5351 SUV in the lateral ventricle superimposed on the coregistered MRI. Color maps and the corresponding color bar (SUVR) depict the decreasing CSF levels of the tracer at 1, 10, 30 and 60 min.

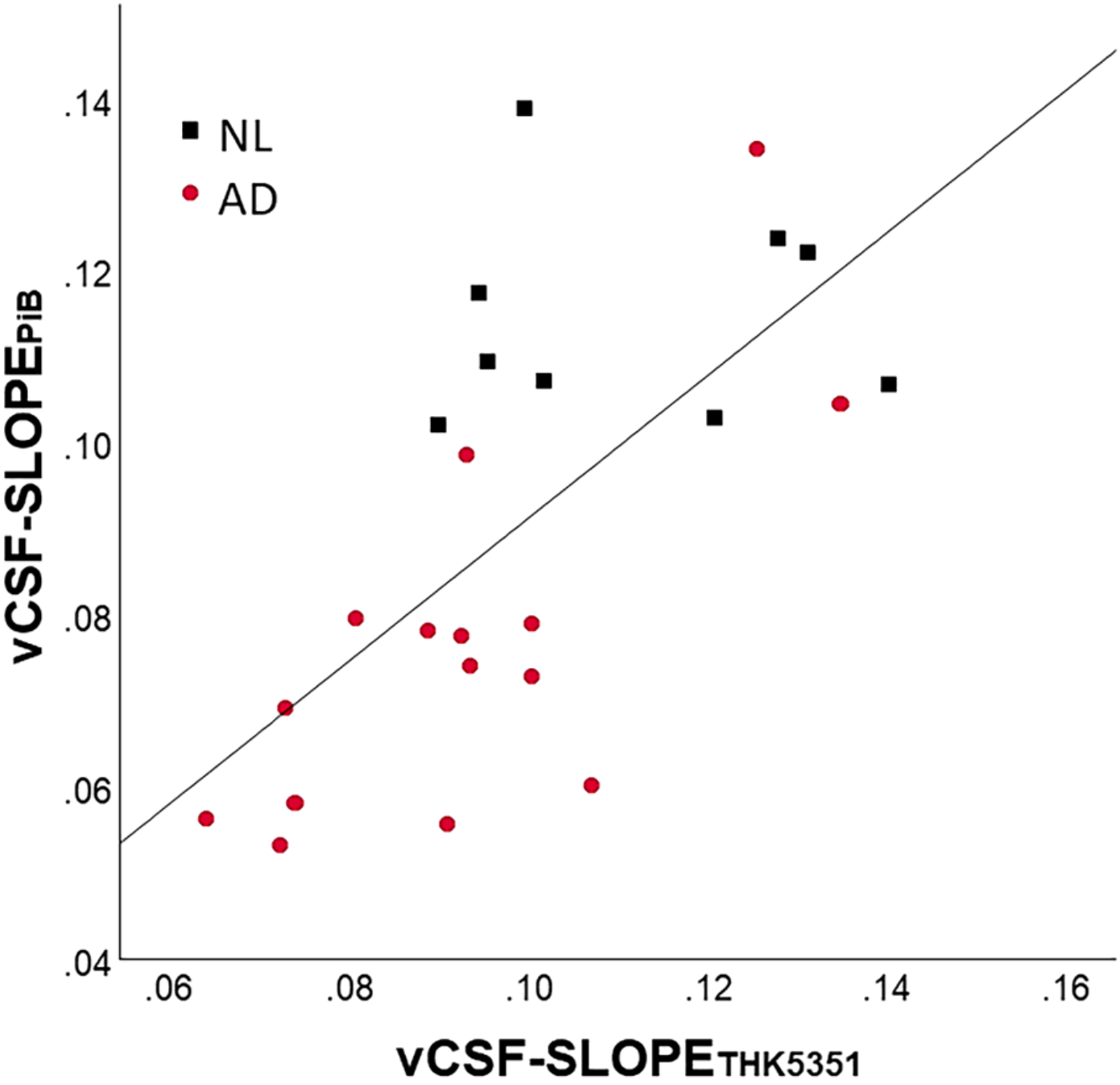

Figure 2

Cross-tracer agreement of clearance: the vCSF-SLOPE for 11C-PiB and the18F-THK5351 tracers are highly correlated (r=.66, p<.01, n=24).

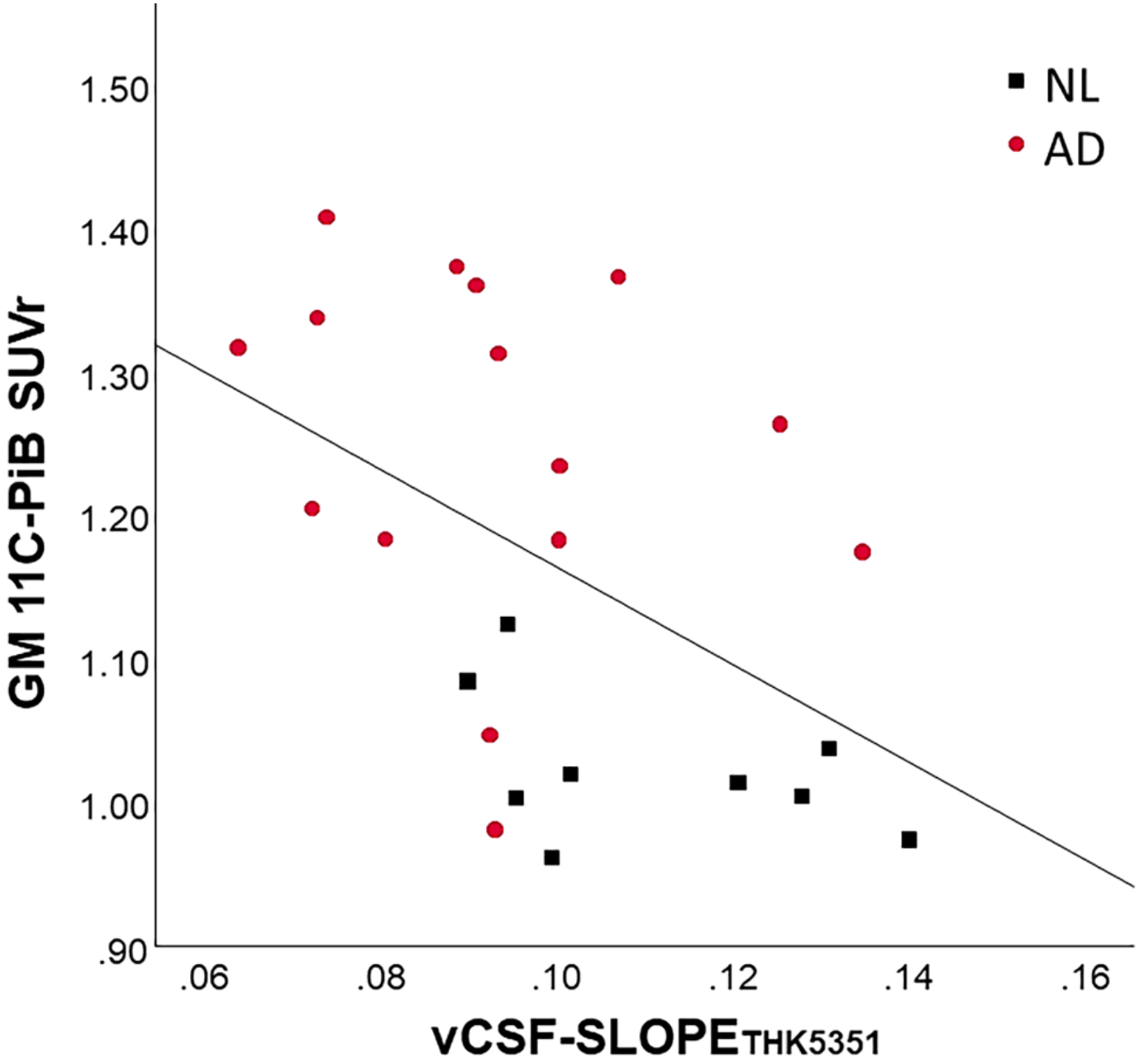

Figure 3

The vCSF-SLOPETHK5351 is inversly correlated with extent of fibrillar Aβ as estimated by PiB GM binding (r=−.64, p<.01, n=24). The correlation remains significant when restricted to the AD group (r=−.58, p<.05, n=15). NL: (black); AD: (red).